ACS APPLIED NANO MATERIALS

www.acsanm.org Article

Nonenzymatic Saliva-Range Glucose Sensing Using Electrodeposited Cuprous Oxide Nanocubes on a Graphene Strip

Wenyu Gao, Xiaojing Zhou,* Nina F. Heinig, Joseph P. Thomas, Lei Zhang, and Kam Tong Leung*

Cite This: *ACS Appl. Nano Mater.* 2021, 4, 4790−4799 Read Online

ACCESS | Metrics & More | Article Recommendations | Supporting Information

ABSTRACT: Cuprous oxide (Cu_2O) nanomaterials provide a versatile platform for building nonenzymatic glucose sensors. In particular, Cu_2O nanocubes with controllable sizes and distributions can be deposited electrochemically on a conductive graphene strip as a soft substrate under different conditions, including overpotential, temperature, copper-ion electrolyte concentration, and deposition time. Graphene provides a promising substrate for sensing because of its high conductivity, high specific surface area, and unique thermal and mechanical properties. A more negative overpotential is found to produce smaller nanocubes with a large number density, while the deposition temperature could affect the morphology of nanocubes. The size of the nanocubes increases with increasing copper-ion concentration and deposition time. Using an optimal condition of −1.0 V vs Ag/AgCl, 1 mM [Cu^{2+}], and 100 s deposition time at room temperature, we obtain a near-homogeneous monolayer of Cu_2O-shell Cu-core nanocubes, ∼50 nm in size, on a graphene strip substrate. The Cu_2O nanocubes/graphene system is used as a high-performance sensor with a wide detection range of 0.002−17.1 mM and a high sensitivity appropriate for saliva-range glucose sensing. It has also been used to test glucose in the real saliva sample with 95% accuracy. This nonenzymatic glucose sensor is considerably better in performance than other nonenzymatic sensors, including those based on bare graphene, and graphene sputter-coated with a Cu film, and conventional enzymatic sensors such as glucose oxidase immobilized on graphene (with and without Nafion). In addition to being an excellent catalyst, Cu_2O nanocubes have a large specific surface area and a large amount of active sites. These nanomaterial properties, along with the use of a high-conductivity substrate like graphene, make the Cu_2O nanocubes/graphene sensor among the best saliva-range glucose sensors reported to date.

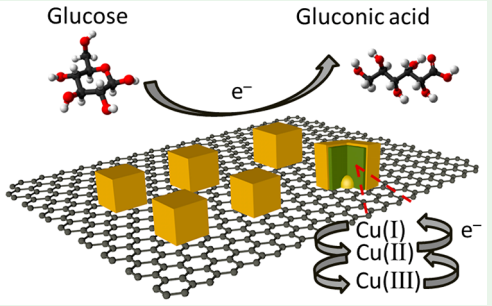

KEYWORDS: *saliva-range, nonenzymatic glucose sensor, electrocatalyst, Cu_2O nanocubes, graphene substrate*

INTRODUCTION

Metal and metal oxide nanoparticles have attracted a lot of attention for decades because of their special electronic, mechanical, and catalytic properties.[1] One prominent example is cuprous oxide nanoparticles, which have been used as a catalyst for biosensors,[2,3] an antifouling coating,[4] an essential component in plasmonics,[5] and other applications (such as amination coupling reactions, antimicrobial coating, food packaging, and drug-delivery applications)[6−8] due to their high conductivity, low toxicity, environment friendliness, and low cost. Compared to other metals, copper has outstanding catalytic properties, and copper-based biosensors show superior performance in sensitivity (with a wide dynamic range), detection limit, stability, and interference-free selectivity.[9] Earlier studies have focused on nonenzymatic glucose biosensors based on copper materials, such as metallic Cu,[10] cupric oxide (CuO),[11] cuprous oxide (Cu_2O),[12] and their composite oxides.[13] Among the many approaches to fabricate copper and copper oxide nanoparticles, such as nanosphere lithography,[14] hydrothermal synthesis,[15] ion implantation,[16] and sonochemical reduction,[17] electrochemical deposition[18] offers a quick, low-cost, and reproducible fabrication method for these nanoparticles. Furthermore, there are also a large variety of substrates readily available for electrodeposition, including silicon,[19] indium tin oxide,[20] and glassy carbon electrode.[21] In addition to these hard substrates, flexible soft substrates are becoming more accessible for depositing copper and copper oxide nanoparticles. Among these, two-dimensional materials such as graphene have been recently used in many areas, including electronics, photonics, and biomedical applications.[22] Several metal and metal oxide nanoparticles (e.g., Pt,[23] Au,[24] Pd,[25] TiO_2,[26] Co_3O_4[27]) have been fabricated on graphene sheets. Indeed, the graphene sheet itself has attracted a lot of commercial interest because of its high electrical conductivity, high specific surface area, and

Received: February 5, 2021
Accepted: May 4, 2021
Published: May 19, 2021

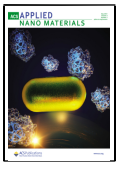

https://doi.org/10.1021/acsanm.1c00381
ACS Appl. Nano Mater. 2021, 4, 4790−4799

unique thermal and mechanical properties.[28] The graphene sheet is therefore a versatile flexible substrate with exceptional conductivity for electrodeposition of copper oxide nanoparticles.

According to the International Diabetes Federation, the number of diabetes patients is expected to increase from 382 million in 2011[29] to 422 million in 2020 and to 642 million in 2040 globally.[30] To monitor the glucose level in a diabetes patient, there are numerous products developed for glucose sensing in the marketplace and even more studies about further improvement to these products. However, most of these products require a blood test from a fingertip, which is an invasive procedure, especially when the patient needs continuous monitoring.[31] There is great interest in developing a totally painless method, other than just changing the blood sample acquisition site from the forearm, thigh, and hand to the finger.[32] Compared to a blood glucose test, saliva glucose analysis has many advantages, including easy-to-collect test samples and less stress for the patient requiring frequent testing throughout the day.[33] While normal glucose concentration in saliva is very low, a significant increase of glucose in saliva in a diabetes patient has been reported.[34] The concentration of glucose in saliva ranges from ∼20 μM in normal subjects to as high as 200 μM in diabetes patients.[34,35] Recently, there has been an accelerated effort in developing noninvasive saliva-range glucose sensors for both enzymatic and nonenzymatic sensing.[36] These include the enzymatic on-chip electrochemical device,[33] the paper strip-based color pH indicator,[37] and glucose sensing electrodes attached on the surface of a mouthguard with a wireless measurement system,[38] as well as the nonenzymatic electrochemical glucose sensor.[39] The mechanism of glucose detection in an enzymatic sensor is different from that of a nonenzymatic one. Generally, the enzymatic glucose monitor depends on the oxidation reaction between the enzyme glucose oxidase (GOx) and glucose through the movement of electrons that generates the current or voltage measured by the electrodes.[40] The overall mechanism follows the well-known reaction of glucose oxidase

$$\mathrm{GOx(FAD)} + \mathrm{glucose} \rightarrow \mathrm{gluconolactone} + \mathrm{GOx(FADH_2)}$$

where GOx (FAD) is the oxidized form of GOx, while GOx ($FADH_2$) is the reduced form.[41] In the case of a metal oxide nanoparticle nonenzymatic sensor, the metal oxide nanoparticle serves as an electrocatalyst to transfer the electrons arising from oxidizing glucose. For instance, the nonenzymatic sensor based on Cu_2O nanoparticles involves transferring electrons from the metal nanoparticles to glucose through the following mechanism. Cu(I) of Cu_2O is electro-oxidized to Cu(II) species, i.e., $Cu(OH)_2$, which is further oxidized to Cu(III) species, i.e., (CuOOH), in the alkaline solution. Glucose is then oxidized to gluconic acid, while Cu(II) and Cu(III) are reduced back to Cu(I). During this process, Cu(III) works in effect as an electron-transfer mediator.[42,43]

$$\mathrm{Cu_2O} + 2\mathrm{OH^-} + \mathrm{H_2O} \rightarrow 2\mathrm{Cu(OH)_2} + 2\mathrm{e^-}$$

$$\mathrm{Cu(OH)_2} \rightarrow \mathrm{CuO} + \mathrm{H_2O}$$

$$\mathrm{CuO} + \mathrm{OH^-} \rightarrow \mathrm{CuOOH} + \mathrm{e^-}$$

$$\mathrm{CuOOH} + \mathrm{glucose} \rightarrow \mathrm{Cu(OH)_2} + \mathrm{gluconic\ acid}$$

In the present work, we fabricate a high-performance nonenzymatic glucose sensor for noninvasive saliva-range glucose testing by taking advantage of the novel properties of Cu_2O nanocubes and the flexible graphene substrate. The Cu_2O nanocubes are deposited using a facile electrochemical method, and the optimum electrodeposition conditions are selected by changing the deposition voltage, electrolyte concentration, deposition time, and temperature.

EXPERIMENTAL DETAILS

All of the chemicals, including copper sulfate, sodium perchlorate, sodium hydroxide, glucose, glucose oxidase, and Nafion, were used as purchased from Sigma-Aldrich. Filtered high-resistivity (18.2 MΩ cm) deionized water was used for preparing all of the solutions. Conductive graphene sheets (25 μm thick), with a sheet resistance of 28 mΩ/square, were purchased from Graphene Laboratories, Inc. and used as substrates. The saliva samples were collected from volunteers based on the requirement of saliva collection and then centrifuged at 12 000 rpm for 10 min to obtain the supernatants, which were collected and stored at 4 °C until use.

All of the electrochemical experiments were conducted in a three-electrode system connected to a CH Instruments 660 electrochemical station, with a Ag/AgCl reference electrode and a platinum wire counter electrode. The working electrode used for electrochemical deposition of Cu_2O nanoparticles was a graphene strip (10 × 5 mm^2), cut from a graphene sheet. Cuprous oxide was deposited over a typical 5 × 5 mm^2 area of the graphene strip by potentiostatic amperometry for 100 s in a 1 mM copper sulfate ($CuSO_4{\cdot}5H_2O$) electrolyte with 10 mM sodium perchlorate ($NaClO_4$) as the supporting electrolyte. The resulting Cu_2O/graphene sample was then used as the working electrode for nonenzymatic glucose sensing. As a comparison of the Cu_2O/graphene sensing performance, we also prepared three other electrodes: (a) a bare graphene strip, (b) a graphene strip coated with copper for 60 s in a magnetron sputterer, and (c) a graphene strip coated with glucose oxidase (GOx) by adding 40 μL 5 μM glucose oxidase solution and allowing to dry overnight (GOx/graphene). We also added 20 μL 0.5% wt. Nafion to the GOx/graphene sample and allowed it to dry for 3 h at 4 °C (GOx/Nafion/graphene) in an attempt to improve its sensing performance. Details of the testing procedure for glucose are given below. A Zeiss Merlin field emission microscope was used to characterize the surface morphologies by scanning electron microscopy (SEM). Glancing-incidence X-ray diffraction (XRD) to determine the crystal structures was performed in a PANalytical X'Pert Pro MRD diffractometer with Cu Kα (1.542 Å) radiation at an incidence angle of 0.6°. X-ray photoelectron spectroscopy (XPS) conducted in a Thermo-VG Scientific ESCALab 250 microprobe with monochromatic Al Kα radiation (1486.6 eV) and a typical energy resolution of 0.5 eV full width at half-maximum was used to characterize the chemical-state composition. A Zeiss Orion plus helium-ion microscope operated at 40 kV was used to dissect a single Cu_2O nanocube to confirm the core−shell structure. Finally, a commercial blood glucose monitoring system (ACCU-CHEK Aviva, Roche Diagnostics) for capillary, whole blood, amperometric testing using glucose dehydrogenase coated test strips was used to determine the blood glucose concentrations of human subjects. These results were used as a reference to compare with results obtained from our salvia-range sensors.

RESULTS AND DISCUSSION

Fabrication of Cuprous Oxide Nanocubes. The cuprous oxide nanocubes are synthesized on a soft high-conductivity substrate graphene strip by one-step, templateless, and capping-agent-free electrodeposition. Cyclic voltammetry shows, in Figure S1 (Supporting Information), two reduction peaks at −0.3 V (Feature A) and −0.6 V (Feature B) and two oxidation features at +0.28 V (Feature A′) and +0.68 V (Feature B′), all with respect to Ag/AgCl, at room temper-

https://doi.org/10.1021/acsanm.1c00381
ACS Appl. Nano Mater. 2021, 4, 4790−4799

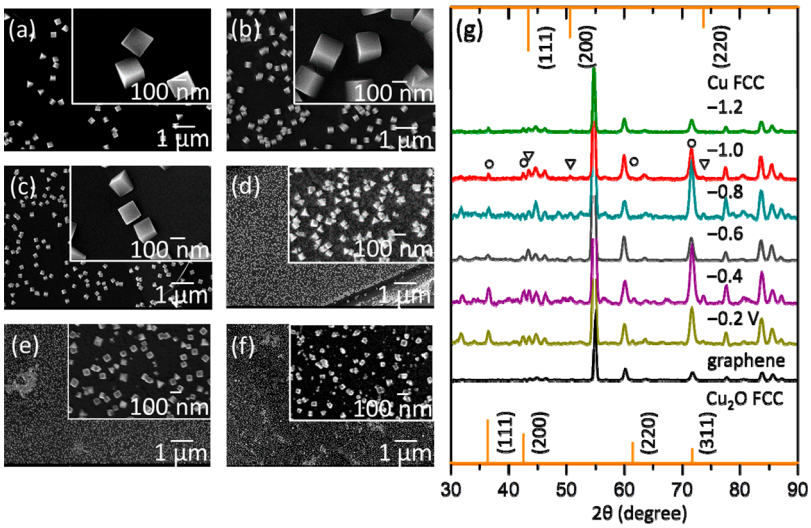

Figure 1. SEM images of Cu_2O nanocubes electrodeposited at (a) −0.2 V, (b) −0.4 V, (c) −0.6 V, (d) −0.8 V, (e) −1.0 V, and (f) −1.2 V (all with respect to Ag/AgCl) in 1 mM $CuSO_4{\cdot}5H_2O$ and 10 mM $NaClO_4$ at room temperature for 100 s. (g) Corresponding glancing incidence X-ray diffraction profiles are assigned in accordance with the reference profiles for the Cu face-centered cubic (FCC) phase (JCPDS 01-070-3039), marked by triangles, and Cu_2O FCC phase (JCPDS 03-065-3288), marked by circles, along with the measured profile for a pristine graphene substrate.

ature. Deposition performed at an overpotential more negative than −0.3 V is found to produce small metal nanoparticles. In accord with the nucleation mechanism, the nucleus number density tends to be higher with increasingly more negative overpotential.[44,45] Figure 1a−f shows the typical morphologies of nanocubes obtained by potentiostatic amperometry at different overpotentials in a 1 mM Cu^{2+} electrolyte solution for 100 s deposition time (all conducted at room temperature). Evidently, the deposited Cu_2O nanocubes are found to be nearly of the same size and uniformly distributed on the conductive graphene substrate. The size of Cu_2O nanocubes becomes smaller while the number density becomes larger when more negative overpotentials are employed. For the 100 s deposition, Cu_2O nanocubes with the largest number density are obtained at −1.2 V and they appear to have the smallest size (40 nm side length, Figure 1f), while the Cu_2O nanocubes obtained at −0.2 V have the largest size (220 nm side length) with the least density (Figure 1a).

The morphology and size of the nanodeposits also depend on other deposition parameters, including the deposition temperature, electrolyte concentration, and deposition time. The deposition temperature could influence the electrochemical thermodynamics and kinetics.[46] Figure S2 (Supporting Information) shows that the nanocubes appear to increase in size with increasing deposition temperature, from 20 nm at 40 °C to 30 nm at 60 °C to 80 nm at 70 °C. The temperature of the electrolyte solution directly affects the viscosity of the solution and consequently the diffusion coefficient and the thickness of the diffusion layer.[47] The electrolyte concentration also has an important effect on the morphology of the nanocubes. A higher Cu^{2+} concentration leads to a larger nucleus size and to larger nanocubes at the expense of the number density. Since the size of the nucleus determines the extent of its diffusion zone, the size of a nanocube is proportional to the size of the nucleus. The size of the nanocubes is found to increase with increasing Cu^{2+} concentration at the same overpotential (Figure S3, Supporting Information). Among the possible nanoparticle shapes, such as cubic, cuboctahedral, and octahedral, that could be obtained on a silicon substrate, a low Cu^{2+} concentration (about 10 mM) tends to favor nanocubes.[48] As graphene is more conductive than the Si substrate, nanocubes with a size range of 15−250 nm can be deposited with an even lower Cu^{2+} concentration (below 10 mM). Figure S4 (Supporting Information) shows the morphology change of the nanocubes obtained at −1.0 V in a 5 mM Cu^{2+} solution with increasing deposition time from 1, 10, 50, and 100 to 200 s. Cu_2O nanocubes generally increase in size with a longer deposition time because of the increase in the amount of electron transfer. Figure S5 (Supporting information) shows the morphology change of the nanocubes obtained in a 1 mM Cu^{2+} solution, in which the increasing trend in the size with increasing time is not as obvious as shown in Figure S4 (i.e., at a higher concentration). In addition to the growth in the nanocube size, the emergence of nanodendrites is evident at a larger deposition time with the present (Figure S4, Supporting Information) and higher electrolyte concentrations. As the Cu_2O nanocubes become larger, they are in contact with one another, forming linear chains.[49,50] These studies enable us to synthesize and deposit Cu_2O nanocubes on a graphene substrate without the need for employing templates and capping agents by simply using potentiostatic amperometry.[48] As shown in our XRD and XPS data below, the Cu_2O nanocubes so produced are found to be core−shell particles. The nature of the electrode material and the crystallographic orientation of the surface determine the value of zero-charge potential. The conductive graphene strip used as the substrate in the present work provides notable advantages for electrodeposition including high charge carrier mobility, excellent thermal conductivity, mechanical flexibility, and large specific surface area. For glucose sensing, nanocubes of 50 nm in size are used because a uniformly distributed, near-monolayer coverage of Cu_2O nanocubes can be obtained on a graphene substrate, by the aforementioned facile electrodeposition at −1.0 V in 1 mM $CuSO_4{\cdot}5H_2O$ and 10 mM $NaClO_4$ for 100 s at room temperature (Figure 1e).

The corresponding glancing incidence X-ray diffraction profiles of Cu_2O nanocubes deposited at different over-

https://doi.org/10.1021/acsanm.1c00381
ACS Appl. Nano Mater. 2021, 4, 4790−4799

potentials are shown in Figure 1g. The strongest peak at 54.72° corresponds to the graphene substrate, and all of the XRD profiles are normalized to this graphene peak. The primary peaks corresponding to Cu and Cu_2O are marked by triangles and circles, respectively. For the nanocubes deposited at −1.0 V vs Ag/AgCl, the prominent peaks at 36.50 and 42.40° are in good accord with the respective (111) and (200) planes of the Cu_2O face-centered cubic phase, while the weaker features at 61.52 and 73.69° correspond to the (220) and (311) planes (JCPDS 03-065-3288). The discernibly weaker features at 43.34, 50.47, and 74.17° can be attributed, respectively, to the (111), (200), and (220) planes of the Cu face-centered cubic phase (JCPDS 01-070-3039). The presence of both Cu_2O and Cu features suggests a core−shell nanostructure for the nanocube, which is also supported by the depth-profiling X-ray photoelectron spectra discussed below. As the relative diffraction intensities of the Cu_2O features appear higher than those of the Cu features, the Cu_2O shell could therefore be quite substantial relative to the Cu core. The XRD profiles for nanocubes with different sizes obtained at different overpotentials shown in Figure 1g are found to be similar, which suggests similar crystallography for these core−shell nanocubes with different sizes.

Figure 2a shows the corresponding XPS spectra of the Cu 2p and O 1s regions of the Cu_2O nanocube samples presented in Figure 1. In addition to the prominent Cu $2p_{3/2}$ (Cu $2p_{1/2}$) peak at 932.3 eV (952.1 eV) attributed to Cu_2O or Cu, a weaker Cu $2p_{3/2}$ (Cu $2p_{1/2}$) feature at 934.2 eV (954.3 eV) and its shake-up satellite features at 940.0-943.5 eV can be assigned to CuO.[51−53] The relative intensity of the Cu $2p_{3/2}$ peak for Cu_2O/Cu with respect to that for CuO appears larger for the Cu_2O nanocubes obtained at −1.0 V (and −1.2 V) than those for nanocubes deposited at less negative overpotentials. This indicates that the relative proportion of Cu_2O/Cu in the smaller nanocubes obtained at −1.0 V (and −1.2 V) is more than the larger nanocubes obtained at the less negative overpotentials. The two O 1s peaks at 530.5 and 531.9 eV in the corresponding O 1s spectra are assigned to Cu_2O/CuO and −OH bond, respectively. The presence of CuO is consistent with the easy oxidation of Cu_2O nanoparticles to CuO in water or in air.[54] The −OH bond feature can be attributed to the presence of hydroxyl group on the graphene substrate after electrodeposition because of water adsorption.

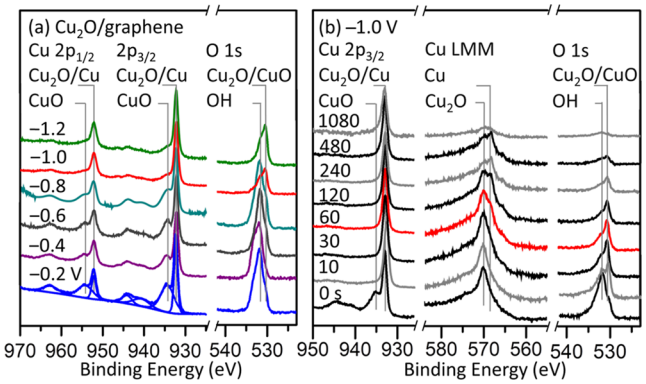

Figure 2. XPS spectra of (a) Cu $2p_{3/2}$ and Cu $2p_{1/2}$, and O 1s regions of Cu_2O nanocubes electrodeposited on graphene at different overpotentials in 1 mM $CuSO_4 \cdot 5H_2O$ and 10 mM $NaClO_4$ at room temperature for 100 s. (b) Corresponding depth-profiling XPS spectra of the Cu $2p_{3/2}$ photopeak, Cu LMM Auger peak, and O 1s regions of the Cu_2O nanocubes obtained at −1.0 V vs Ag/AgCl in (a).

While the Cu 2p photopeaks for CuO and Cu_2O/Cu can be easily discerned in Figure 2a, the relative locations of the CuO and Cu_2O/Cu components in the nanocube are less clear. Furthermore, it is difficult to identify the presence of metallic Cu because the metallic Cu feature (at 932.8 eV) is separated in binding energy from the Cu_2O feature at 932.9 eV by only 0.1 eV (i.e., considerably smaller than the instrumental resolution of our XPS system).[55] In Figure 2b, we show the depth-profiling XPS spectra of the Cu $2p_{3/2}$ photopeak, Cu $L_3M_{45}M_{45}$ Auger peak, and O 1s photopeak regions of the nanocubes/graphene sample obtained at −1.0 V as a function of Argon sputtering time. The CuO Cu 2p and OH O 1s features appear to be easily removed by brief sputtering. After 10 s sputtering of the Cu_2O nanocubes, the weaker CuO Cu $2p_{3/2}$ feature at 934.2 eV appears to have been removed completely, which indicates that CuO exists as a thin outermost layer on the surface of the nanocubes. After 60 s sputtering of the Cu_2O nanocubes, a weak Cu LMM peak at 568.6 eV corresponding to metallic Cu emerges at the low binding energy side of the prominent Cu_2O Cu LMM peak at 570.1 eV. The relative intensity of this metallic LMM feature becomes stronger upon further sputtering for a total of 240 s, confirming the presence of the metallic core in the nanocubes. In addition, the Cu $2p_{3/2}$ peak at 932.3 eV and Cu LMM peak at 570.1 eV for Cu_2O remain prominent upon further sputtering. This suggests that Cu_2O is the main component of the nanocubes. As depicted in a schematic diagram in Figure 3b, these depth-profiling XPS data therefore show that the

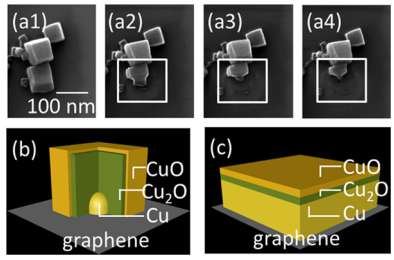

Figure 3. (a1−a4) Helium-ion micrographs of an individual nanocube (marked by an open square) in a cluster of Cu_2O nanocubes (electrodeposited on a graphene substrate at −1.0 V in a 1 mM $CuSO_4 \cdot 5H_2O$ and 10 mM $NaClO_4$ solution for 100 s at room temperature) upon sequential scanning (and sputtering) with a helium-ion beam. Schematic models of the proposed structures of (b) a Cu_2O nanocube on graphene and (c) a Cu film sputter-coated on graphene.

Cu_2O nanocube consists of a small metallic Cu core, a prominent Cu_2O shell, and a thin CuO skin (as the outermost layer). Similarly, the strong O 1s peak at 531.9 eV is greatly reduced after sputtering for 10 s, and it becomes totally diminished after 60 s of sputtering, which suggests that this OH feature is on the surface of the graphene substrate. The O 1s shoulder remaining after further sputtering corresponds to water adsorption of graphene substrate which is not covered by Cu_2O nanocubes.

To confirm the core−shell model of an individual Cu_2O nanocube, we take advantage of the nanoscale probing capability of helium-ion microscopy. Figure 3a1 shows a helium-ion micrograph of a group of nanocubes on graphene before sequential raster-sputtering of one of the nanocubes

https://doi.org/10.1021/acsanm.1c00381
ACS Appl. Nano Mater. 2021, 4, 4790−4799

with the helium-ion beam, as marked by the open square in Figure 3a2−a4. After the first scanning of the area inside the open square, removal of about half the nanocube is evident and a T-shape object appears in Figure 3a2, which indicates that the shell/perimeter of the nanocube is removed more efficiently than its core portion. This suggests that the material on the perimeter and the core are chemically different, with the former, likely softer, material appearing to be more easily sputtered away than the harder core material during the scanning with the high-energy helium-ion beam. Continued scanning (and sputtering) of the same area with the helium-ion beam ultimately removes the harder core material, as shown in Figure 3a3,a4. While these helium-ion images do not identify the chemical nature of the components, they illustrate the material difference between the shell and the core of a single nanocube. Combining with the depth-profiling XPS data shown in Figure 2b therefore supports our proposed model of the Cu_2O nanocube to consist of a Cu core, a Cu_2O shell, and a CuO skin, shown in Figure 3b. For comparison, we also show a schematic model of a sputter-coated Cu film on graphene in Figure 3c, which consists of a Cu film on top of graphene with a Cu_2O overlayer and a CuO outermost layer.

Glucose Sensing Performance of Cu_2O Nanocubes/Graphene and Related Graphene Sensors. To date, the most common commercial products for glucose sensing in the marketplace are enzymatic glucose sensors. Generally, this type of commercial glucose sensors is popular because of its high selectivity to the target molecule, glucose. Enzyme immobilization can be commonly achieved by direct adsorption, sol−gel adsorption, and cross-linking.[56] One major challenge for enzymatic biosensors is the stability of the enzyme over long-term storage because the activity of the enzyme could be affected by the temperature, pH, humidity, and ionic strength.[57] This potential issue provides an opportunity for nonenzymatic biosensors, in which glucose is oxidized on the surface of the electrode to generate the current directly without the need for enzyme immobilization. The entire process occurs at the active sites of the electrode where the glucose molecules are adsorbed. In addition to low cost and good stability, copper oxides work as the electrocatalysts in a glucose sensor because of their high electro-oxidation activity and their propensity for electron-transfer reactions at low overpotential.[58,59] In the present work, the active sites of the glucose sensor are provided by the Cu_2O nanocubes electrodeposited on the graphene substrate at −1.0 V in a 1 mM $CuSO_4{\cdot}5H_2O$ (electrolyte) and 10 mM $NaClO_4$ (supporting electrolyte) solution for 100 s at room temperature. The average size of these Cu_2O nanocubes so produced is 50 nm (Figure 1e). These deposition conditions provide on graphene a large density of Cu_2O nanocubes of a small size of a near-monolayer coverage that is optimal for use as a catalyst.

To investigate the efficacy of this Cu_2O nanocubes/graphene sensor, we compare its glucose sensing performance with three other sensors: a bare graphene strip (graphene), a graphene strip coated with a copper film by magnetron sputtering for 60 s (Cu/graphene), and an enzymatic sensor based on glucose oxidase (GOx) immobilized on a graphene strip without (GOx/graphene) and with Nafion (GOx/Nafion/graphene). With the increase of glucose concentration (0−2.4 mM), the distinct enlargements of the redox current signal are obtained and the potential for current vs time curves is selected at 0.6 V vs Ag/AgCl as shown in Figure S6. Figure 4 shows the characteristic current vs time (or $i-t$) curves at 0.6 V vs Ag/AgCl upon stepwise addition of an aliquot of 20 μL glucose (of 10 mM concentration), with constant stirring, to these sensors immersed in a 10 mL 0.1 M NaOH solution. The reason why Cu_2O nanocubes/graphene sensor needs to work in NaOH solution is due to the catalysis mechanism of Cu_2O as mentioned above, in which Cu(I) is to be oxidized to Cu(II) forming $Cu(OH)_2$, and to be further oxidized to CuOOH. For this reason, the detection should be performed under alkaline condition. We have also attempted the detection in PBS (with pH 7) and confirm that Cu_2O nanocubes do not work as a catalyst for glucose if we do not add the NaOH base. The corresponding SEM images of the sensors before the addition of glucose are also shown. For the bare graphene sensor, the current jump is small upon glucose addition and its linear range is 0.02−1.10 mM with a sensitivity of 1.90 μA mM^{-1} cm^{-2} (Figure 4a1). Even though the graphene substrate has good conductivity, graphene itself does not produce a large electrical current after glucose addition, making graphene more appropriate as a catalyst support material and not the catalyst itself.

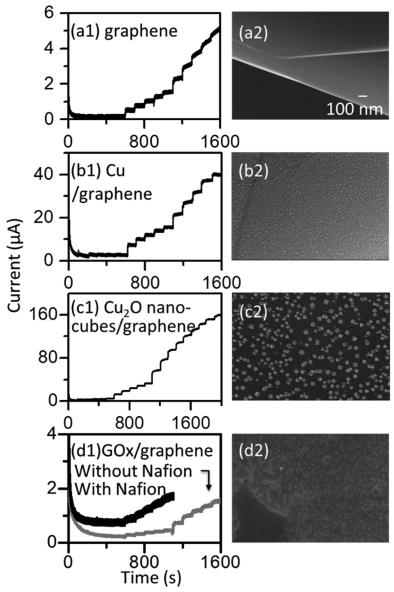

Figure 4. $i-t$ curves (left column) obtained upon sequential addition of aliquots of glucose to 0.1 M NaOH at 0.6 V vs Ag/AgCl and the respective SEM images (right column) of (a1, a2) graphene, (b1, b2) Cu/graphene, (c1, c2) Cu_2O nanocubes/graphene, and (d1, d2) GOx/graphene without and with Nafion. The scale bars for all of the SEM images (a2−d2) are the same.

For the Cu/graphene sensor, the corresponding XRD and XPS data in Figure S7 (Supporting Information) show that the sputtered-coated Cu film on graphene undergoes ambient oxidation in air. In Figure S7a, the prominent XRD peaks at 43.31, 50.44, and 74.12° correspond to the (111), (200), and (220) planes of the Cu face-centered cubic phase (JCPDS 01-089-2838). The Cu film does not exhibit any discernible feature of Cu_2O FCC phase (JCPDS 03-065-3288) and CuO monoclinic phase (JCPDS 01-089-2529) because Cu_2O and CuO resulting from oxidization in air might be amorphous or poorly crystalline. In contrast, since Cu_2O nanocubes/graphene has a more crystalline structure with better active sites for electron transfer, the sensor performance is expected to be better. Using the more surface-sensitive XPS technique, we show in Figure S7b (Supporting Information) the presence of Cu_2O/Cu and CuO in the Cu-coated graphene, with

https://doi.org/10.1021/acsanm.1c00381
ACS Appl. Nano Mater. 2021, 4, 4790−4799

photopeaks at their respective binding energy positions as those indicated for the Cu_2O nanocubes/graphene sample in Figure 2b. Depth-profiling XPS spectra of the Cu LMM Auger region further reveal the presence of metallic Cu (Figure S7b, Supporting Information), the intensity of which increases with increasing sputtering time. On the other hand, the Cu_2O Cu LMM feature is found to decrease with further sputtering for 480 s, which indicates that only the surface of the sputter-coated Cu film reacts with oxygen forming the Cu_2O/CuO overlayer. After sputtering for 1080 s, the prominent composition of Cu/graphene is metallic Cu. In addition, we also anneal the Cu_2O nanocubes sample at 300 °C for 3 h to obtain predominantly CuO. The corresponding XRD profiles and $i-t$ curves for Cu_2O nanocubes and the annealed (i.e., CuO) sample are compared in Figure S8, Supporting Information.

Like the structural composition of the Cu_2O nanocubes on graphene, the Cu_2O/CuO overlayer of the Cu film on graphene works as a catalyst in the oxidation reaction with glucose. The resulting detection range of the Cu/graphene sensor (Figure 4b1) is greatly extended by nearly 10-fold (with respect to the graphene substrate, Figure 4a1) to 0.02−11.10 mM with a sensitivity of 9.56 μA mM^{-1} cm^{-2}. For the Cu_2O nanocubes deposited on graphene (Figure 4c1), the dynamic range for linear detection is found to be even wider and significantly extended over five decades to 0.002−17.100 mM. The linear range of the CuO sample (obtained by annealing) is found to be 0.02−14.66 mM, which is less than that of the Cu_2O nanocubes (Figure S8, Supporting Information). Unlike the sputter-coated Cu film, the Cu_2O nanocubes provide increased catalytic effects through their active sites over a large specific surface area. Finally, the detection range of the enzymatic sensor GOx/graphene without Nafion (Figure 4d1) is found to be quite limited at 0.2−1.0 mM with a sensitivity of 2.86 μA mM^{-1} cm^{-2}, but it can be extended to 0.02−11.10 mM with a sensitivity of 5.60 μA mM^{-1} cm^{-2} by adding 20 μL 0.5% Nafion. In Figure S9 (Supporting Information), we compare the Nyquist plots and the relevant resistances determined for the four sensors. Figure S10 (Supporting Information) provides the corresponding linear curves for these substrates. Evidently, the charge-transfer resistance is found to be the smallest for the Cu/graphene system, followed by those of Cu_2O nanocubes/graphene, graphene, and GOx/graphene. Since the sputter-coated Cu film and electrodeposited Cu_2O nanocubes are considered metallic contact points on graphene, the charge-transfer resistance is smaller than the bare graphene. The presence and availability of reactive sites on Cu_2O nanocubes appear more important for the sensing performance even though Cu/graphene has a lower charge-transfer resistance.

As the glucose sensor is designed for saliva-range glucose sensing, the linear range should be high enough to cover the glucose range for saliva. Figure 5a clearly demonstrates the current jumps upon addition of a sufficiently low concentration of glucose from 2 to 210 μM, which is comparable to the glucose concentration of saliva (20−200 μM) found in normal individuals and diabetes patients.[34,35] Figure 5b shows the linear calibration curve of current vs glucose concentration appropriate for saliva-range glucose sensing. The regression equation for the low concentration of glucose detection gives an R^2 of 0.994. The sensitivity of glucose for the Cu_2O nanocubes/graphene sensor is 36.40 μA mM^{-1} cm^{-2} in this

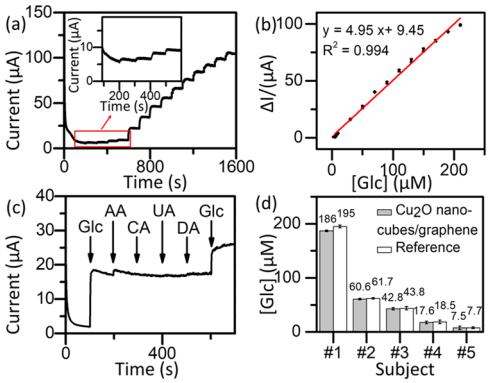

Figure 5. (a) $i-t$ curve upon sequential addition of aliquots of glucose (Glc) with increasing concentration from 2 to 210 μM to the Cu_2O nanocubes/graphene sensor held at 0.6 V vs Ag/AgCl in 0.1 M NaOH and inset shows an expanded view for the 2 to 10 μM concentration range. (b) the corresponding linearity response curve. (c) $i-t$ curve illustrating minimal current jumps due to interference upon adding aliquots of 0.1 mM ascorbic acid (AA), 0.1 mM citric acid (CA), 0.1 mM uric acid (UA), and 0.01 mM dopamine (DA) solutions to 0.1 M NaOH at 0.6 V vs Ag/AgCl. An aliquot of 0.1 mM glucose solution is also added before and after the interference test. (d) Comparison of salvia glucose concentrations derived from blood glucose measurements (right bars) with those obtained using Cu_2O nanocubes/graphene sensor (left bars) for five human subjects.

linear range of 2−210 μM, well above that required for saliva-range glucose sensors.

We also examine the effects of possible interfering species to evaluate the selectivity of the Cu_2O nanocubes/graphene sensor. The physiological level of glucose (3−8 mM) is much higher than those of common interferents such as ascorbic acid (~0.1 mM) and uric acid (~0.02 mM).[60] Furthermore, saccharides such as sucrose and fructose could also be considered as interferents. As sucrose is a disaccharide, it must be broken down into glucose and fructose before the human body could use it. The serum concentration for fructose in diabetes patients has been reported to be 12.0 ± 3.8 μM while that of glucose is above 11 mM.[61] The difference in the relative concentrations of fructose and glucose is therefore about 1000 times in the human body, which allows us to safely neglect the presence of sucrose and fructose as interferents. Using the Cu_2O nanocubes/graphene electrode as the working electrode for amperometry at +0.6 V vs Ag/AgCl, we add a 0.1 mM glucose followed by those of other interferents, including ascorbic acid, citric acid, uric acid, all with 0.1 mM concentration (i.e., at least 10 times higher than the expected level), and dopamine at 0.01 mM, into 20 mL of 0.1 M NaOH. Evidently, ascorbic acid and dopamine yield less than 10% change in the current response compared with the current change of first addition of glucose, while the other interferents (citric acid and uric acid) do not register a response in the $i-t$ curve (Figure 5c).

The stability of the sensor is another important performance metric of a glucose sensor. To observe the relationship between the performance of the Cu_2O nanocubes/graphene sensor over time, we plot the $i-t$ curve after storing a freshly made sensor under ambient conditions for 90 and 180 days and the overlapping linear fitting graph, shown in Figure S11c,d (Supporting Information), respectively. Evidently, the Cu_2O nanocubes/graphene sensor remains functional and stable for at least 180 days. We have also used the same sensor

https://doi.org/10.1021/acsanm.1c00381
ACS Appl. Nano Mater. 2021, 4, 4790−4799

Table 1. Comparison of Saliva-Range Glucose Sensors

electrode matrix	sensitivity (μA mM^{-1} cm^{-2})	limit of detection (μM)	linear range (mM)	applied potential vs Ag/AgCl (V)	reference
bare graphene sheet	1.90	N/A	0.02−1.00	0.6	this work
Cu-coated graphene	9.56	N/A	0.02−11.1	0.6	this work
Cu_2O nanocubes on graphene sheet	36.40	0.23	0.002−17.100	0.6	this work
glucose oxidase on graphene sheet	2.86	N/A	0.2−1.0	0.6	this work
nanospindle-like Cu_2O/straight multiwalled carbon nanotube hybrid nanostructures	2143	0.2	0.0005−2.5	0.4	63
Cu/Cu_2O hollow microspheres	33.63	0.05	0.22−10.89	0.45	66
coral-like PtAu-MnO_2 binary nanocomposites on graphene paper	58.54	20	0.1−30.0	0	67
graphene wrapped Cu_2O nanocubes	N/A	3.3	0.3−3.3	0.6	68
filter paper strip for salivary analysis	N/A	1230	0.50−74.9	N/A	37
Cu_2O nanoparticles on reduced graphene oxide	185	0.05	0.01−6	0.6	42
single-walled carbon nanotubes and multilayers of chitosan, gold nanoparticles, and glucose oxidase on chip saliva nano-biosensor	26.6	5	0.1017−1.11	0.2	69
three-dimensional Cu foam-supported single-crystalline mesoporous Cu_2O nanothorn arrays	97.9	0.005	N/A	0.55	70
Cu_xO/Cu nanowire array	1210	10	0.01−7	0.6	64
sandwich nanoporous framework decorated with vertical CuO nanowire arrays	1950	1	0.1−6	0.58	65

and repeated the detection experiments multiple times. We find that the currents in repeated consecutive tests (using the same sensor) appear to become smaller after each test. We therefore believe that the first test result is the most reliable and our sensor should therefore be considered for one-time detection and not reusable.

To demonstrate the application of our Cu_2O nanocubes/graphene sensor under real biomedical conditions, we obtain blood and saliva samples following Ethics Protocol (approved Application #43115) from five volunteers, four of whom are normal subjects while the fifth is considered prediabetics. Using a commercial amperometric blood glucose testing system with blood deposited on glucose dehydrogenase coated test strips, we determine the blood glucose concentrations of our human subjects. A regression relation ([serum glucose (mg/dL)] = 95.607 + 27.710 [saliva glucose (mg/dL)])[62] is then used to convert the serum or blood glucose concentration to saliva glucose concentration. These reference values of saliva glucose concentrations are shown in Figure 5d. We also collect saliva samples from our human subjects and use our Cu_2O nanocubes/graphene sensor to obtain the respective saliva glucose concentrations by making use of the calibration curve shown in Figure 5b. After centrifuged at 12 000 rpm for 10 min, an aliquot of 200 μL saliva supernatant is added into 10 mL of 0.1 M NaOH, and this solution is then used for amperometry at +0.6 V vs Ag/AgCl. These results are compared with our reference values in Figure 5d. For our prediabetics subject (Subject #1) with a blood glucose concentration of 10.8 mM, corresponding to a derived saliva glucose concentration of 195 μM, our Cu_2O nanocubes/graphene sensor provides a value of 186 μM. For our normal subjects, with blood glucose concentrations of 7.0 mM (Subject #2), 6.5 mM (Subject #3), 5.8 mM (Subject #4), and 5.5 mM (Subject #5), saliva testing using our Cu_2O nanocubes/graphene sensor gives saliva glucose concentrations of 60.6, 42.8, 17.6, and 7.5 μM, respectively. Evidently, there is a clear correlation between blood glucose concentration and saliva glucose concentration. Furthermore, our Cu_2O nanocubes/graphene sensor results are in excellent agreement (better than 95%) with our reference values (derived from blood glucose measurement). The present human subject study (Figure 5d) therefore confirms the high accuracy of saliva glucose testing provided by our Cu_2O nanocubes/graphene sensor. It is also of interest to note that the present saliva glucose sensor results appear to magnify the minor difference in the blood glucose concentrations found in our normal subjects. The saliva glucose sensor results are therefore more sensitive to changes in the blood glucose concentration.

Table 1 summarizes the performance of these four sensors and compares them with other nonenzymatic and enzymatic glucose sensors that are mostly based on Cu_2O nanomaterials. Given that our target linear range of detection for glucose should be 0.02−0.2 mM, all three of our nonenzymatic graphene sensors appear viable for saliva-range glucose detection. Not only is the linear range the widest, the sensitivity of the Cu_2O nanocubes/graphene sensor is also higher than the other two nonenzymatic sensors. The enzymatic GOx/graphene sensor (with and without Nafion) appears less competitive in both sensitivity and linear range performance than even the nonenzymatic Cu/graphene sensor. Several sensors shown in Table 1 have very high sensitivities, e.g., 2143 μA mM^{-1} cm^{-2} for the nanospindle-like Cu_2O/straight multiwalled carbon nanotube hybrid nanostructures,[63] 1210 μA mM^{-1} cm^{-2} for Cu_xO/Cu nanowire array,[64] and 1950 μA mM^{-1} cm^{-2} for the sandwich nanoporous framework decorated with vertical CuO nanowire arrays.[65] The higher sensitivities found for these nanostructures are not unexpected because they all have much higher number densities and therefore much higher amounts of material per unit area. Of the other sensors reported in the literature, only two cover the linear dynamic range of interest. The sensors based on Cu_2O nanoparticles on reduced graphene oxide and on Cu_2O nanospindles on straight multiwalled carbon nanotubes appear to cover the glucose range in saliva and have higher sensitivities. The methods to prepare these sensors are, however, quite elaborate. For instance, Cu_2O nanoparticles

https://doi.org/10.1021/acsanm.1c00381
ACS Appl. Nano Mater. 2021, 4, 4790−4799

are anchored on reduced graphene oxide using an ionic liquid crystal (1-hexadecyl-2,3-dimethylimidazolium bromide) as a template, while Cu_2O nanospindles are fabricated with straight multiwalled carbon nanotubes by a series of (ultra)sonication and heat treatment steps (at different temperatures) before drop-casting onto a glassy carbon electrode to use as a working electrode. The $Cu(OH)_2$ nanograss arrays on uniform nanoporous copper substrate sensor and the sandwiched nanoporous framework decorated with vertical CuO nanowire array sensor have a high sensitivity and a wide range, but they do not cover the range for saliva glucose detection. In our case, Cu_2O nanocubes can be obtained on a commercial graphene strip by facile electrodeposition in an aqueous electrolyte. The resulting Cu_2O nanocubes/graphene sensor provides a wide linear detection range of 0.002−17.100 mM that is comparable to those achieved by other much more complex, less stable, or difficult-to-fabricate sensors. Our graphene strip offers a flexible substrate with good conductivity to transfer electrons, while the near-homogeneous monolayer of Cu_2O nanocubes provides a large specific surface area and numerous reactive sites for nonenzymatic reaction to take place. The present sensor also has good sensitivity and a low limit of detection. The Cu_2O nanocubes/graphene sensor is therefore an excellent candidate for use as a practical and more sensitive saliva-range glucose sensor.

CONCLUSIONS

The size and number density of Cu_2O nanocubes on a graphene substrate have been optimized for use as a saliva-range glucose sensor by changing the electrodeposition overpotential, Cu^{2+} electrolyte concentration, and deposition time at room temperature. The Cu_2O nanocube is found to have a metallic copper core and a Cu_2O shell with a CuO skin as the outermost layer. The glucose sensing performance of this Cu_2O nanocubes/graphene sensor is enhanced by the high conductivity of the graphene substrate and is found to be superior in sensitivity and linear range to other sensors including graphene, graphene sputter-coated with a Cu film, and graphene functionalized with glucose oxidase (with and without Nafion). This Cu_2O nanocubes/graphene sensor exhibits a wide detection range of 0.002−17.1 mM covering the appropriate glucose range found in the saliva in diabetes patients. The sensor is also air-stable, and it remains functional even after storing for 180 days. This sensor has also been tested favorably using real saliva samples. The Cu_2O nanocubes/graphene glucose sensor therefore offers a sensitive noninvasive option for saliva-range glucose monitoring, with minimal interference, for diabetes patients.

ASSOCIATED CONTENT

Supporting Information

The Supporting Information is available free of charge at https://pubs.acs.org/doi/10.1021/acsanm.1c00381.

CV of nanoparticle electrodeposition on a graphene substrate; SEM images of electrodeposits under different conditions of temperature, Cu^{2+} concentration, and deposition time; XRD and XPS profiles of a Cu film on graphene; electrochemical impedance spectroscopy data of four different samples; CV curves of nanocube samples at different glucose concentrations; calibration curves of sensor current responses; and comparison of current responses for Cu_2O nanocubes/graphene sensors after extended storage (PDF)

AUTHOR INFORMATION

Corresponding Authors

Xiaojing Zhou − *School of Mathematical and Physical Sciences, University of Newcastle, Newcastle, New South Wales 2308, Australia*; Email: xiaojing.zhou@newcastle.edu.au

Kam Tong Leung − *WATLab and Department of Chemistry, University of Waterloo, Waterloo, Ontario N2L 3G1, Canada*; orcid.org/0000-0002-1879-2806; Email: tong@uwaterloo.ca

Authors

Wenyu Gao − *WATLab and Department of Chemistry, University of Waterloo, Waterloo, Ontario N2L 3G1, Canada*

Nina F. Heinig − *WATLab and Department of Chemistry, University of Waterloo, Waterloo, Ontario N2L 3G1, Canada*

Joseph P. Thomas − *WATLab and Department of Chemistry, University of Waterloo, Waterloo, Ontario N2L 3G1, Canada*

Lei Zhang − *WATLab and Department of Chemistry, University of Waterloo, Waterloo, Ontario N2L 3G1, Canada*

Complete contact information is available at: https://pubs.acs.org/10.1021/acsanm.1c00381

Notes

The authors declare no competing financial interest.

ACKNOWLEDGMENTS

This work was supported by the Natural Sciences and Engineering Research Council of Canada.

REFERENCES

(1) George, J. M.; Antony, A.; Mathew, B. Metal oxide nanoparticles in electrochemical sensing and biosensing: a review. *Microchim. Acta* **2018**, *185*, 358−384.

(2) Akhavan, O.; Ghaderi, E. Copper oxide nanoflakes as highly sensitive and fast response self-sterilizing biosensors. *J. Mater. Chem.* **2011**, *21*, 12935−12940.

(3) Liu, M.; Zhao, H.; Chen, S.; Yu, H.; Zhang, Y.; Quan, X. A "turn-on" fluorescent copper biosensor based on DNA cleavage-dependent graphene-quenched DNAzyme. *Biosens. Bioelectron.* **2011**, *26*, 4111−4116.

(4) Abiraman, T.; Ramanathan, E.; Kavitha, G.; Rengasamy, R.; Balasubramanian, S. Synthesis of chitosan capped copper oxide nanoleaves using high intensity (30kHz) ultrasound sonication and their application in antifouling coatings. *Ultrason. Sonochem.* **2017**, *34*, 781−791.

(5) Sugawa, K.; Yamaguchi, D.; Tsunenari, N.; Uchida, K.; Tahara, H.; Takeda, H.; Tokuda, K.; Jin, S.; Kusaka, Y.; Fukuda, N.; Ushijima, H.; Akiyama, T.; Watanuki, Y.; Nishimiya, N.; Otsuki, J.; Yamada, S. Efficient photocurrent enhancement from porphyrin molecules on plasmonic copper arrays: beneficial utilization of copper nano-anntenae on plasmonic photoelectric conversion systems. *ACS Appl. Mater. Interfaces* **2017**, *9*, 750−762.

(6) Seung, U. S.; Park, K. I.; Park, J.; Hyeon, T. Synthesis of Cu_2O coated Cu nanoparticles and their successful applications to Ullmann-type amination coupling reactions of aryl chlorides. *Chem. Commun.* **2004**, 778−779.

(7) Zain, N. M.; Stapley, A. G.; Shama, G. Green synthesis of silver and copper nanoparticles using ascorbic acid and chitosan for antimicrobial applications. *Carbohydr. Polym.* **2014**, *112*, 195−202.
(8) Ashfaq, M.; Khan, S.; Verma, N. Synthesis of PVA-CAP-based biomaterial in situ dispersed with Cu nanoparticles and carbon micro-nanofibers for antibiotic drug delivery applications. *Biochem. Eng. J.* **2014**, *90*, 79−89.
(9) Sun, F.; Li, L.; Liu, P.; Lian, Y. F. Nonenzymatic electrochemical glucose sensor based on novel copper film. *Electroanalysis* **2011**, *23*, 395−401.
(10) Wu, H. X.; Cao, W. M.; Li, Y.; Liu, G.; Wen, Y.; Yang, H. F.; Yang, S. P. In situ growth of copper nanoparticles on multiwalled carbon nanotubes and their application as non-enzymatic glucose sensor materials. *Electrochim. Acta* **2010**, *55*, 3734−3740.
(11) Jiang, L. C.; Zhang, W. D. A highly sensitive nonenzymatic glucose sensor based on CuO nanoparticles-modified carbon nanotube electrode. *Biosens. Bioelectron.* **2010**, *25*, 1402−1407.
(12) Yousef, E. M.; Khodadadi, A. A.; Mortazavi, Y. A glucose biosensor based on glucose oxidase immobilized on ZnO/Cu_2O graphene oxide nanocomposite electrode. *J. Electrochem. Soc.* **2014**, *161*, 81−87.
(13) Meng, F.; Shi, W.; Sun, Y.; Zhu, X.; Wu, G.; Ruan, C.; Liu, X.; Ge, D. Nonenzymatic biosensor based on Cu(x)O nanoparticles deposited on polypyrrole nanowires for improving detection range. *Biosens. Bioelectron.* **2013**, *42*, 141−147.
(14) Chan, G. H.; Zhao, C. J.; Erin, M. H.; Geroge, C. S.; Richard, P. V. D. Plasmonic properties of copper nanoparticle fabricated by nanosphere lithography. *Nano Lett.* **2007**, *7*, 1947−1952.
(15) Nathan, D. M. G. T.; Boby, S. J. M.; Prabir, B.; Mahesh, R.; Harish, S.; Shibu, J.; Sagayaraj, P. One-pot hydrothermal preparation of Cu_2O-CuO/rGO nanocomposites with enhanced electrochemical performance for supercapacitor applications. *Appl. Surf. Sci.* **2018**, *449*, 474−484.
(16) Stepanov, A. L.; Khaibullin, I. B. Fabrication of metal nanoparticles in sapphire by low-energy ion implantation. *Rev. Adv. Mater. Sci.* **2005**, *9*, 109−129.
(17) Abulizi, A.; Yang, G. H.; Zhu, J. J. One-step simple sonochemical fabrication and photocatalytic properties of Cu_2O-rGO composites. *Ultrason. Sonochem.* **2014**, *21*, 129−135.
(18) Cui, J. B.; Gibson, U. J. A simple two-step electrodepsition of Cu_2O/ZnO nanopillar solar cells. *J. Phys. Chem. A* **2010**, *114*, 6408−6412.
(19) Kida, T.; Oka, T.; Nagano, M.; Ishiwata, Y.; Zheng, X. G. Synthesis and application of stable copper oxide nanoparticle suspensions for nanoparticulate film fabrication. *J. Am. Ceram. Soc.* **2007**, *90*, 107−110.
(20) Ding, L.; Gao, Y.; Di, J. A sensitive plasmonic copper(II) sensor based on gold nanoparticles deposited on ITO glass substrate. *Biosens. Bioelectron.* **2016**, *83*, 9−14.
(21) Karami, K.; Allafchian, A. R.; Amiri, R.; Shirani, F.; Bayat, P.; Rezaei, B. Glassy carbon electrode modified by new copper(I) oxide nanocomposite for glucose detection: an electroanalysis study. *Appl. Organomet. Chem.* **2019**, *33*, 4834−4842.
(22) Khan, K.; Tareen, A. K.; Aslam, M.; Wang, R.; Zhang, Y.; Mahmood, A.; Ouyang, Z.; Zhang, H.; Guo, Z. Recent developments in emerging two-dimensional materials and their applications. *J. Mater. Chem. C* **2020**, *8*, 387−440.
(23) Si, Y. C.; Samulski, E. T. Exfoliated graphene separated by platinum nanoparticles. *Chem. Mater.* **2008**, *20*, 6792−6797.
(24) Khalil, I.; Wageeh, A. Y.; Nurhidayatullaili, M. J.; Shahrooz, R.; Abu, A. I. S.; Wan, J. B.; Mohd, R. J. Graphene oxide and gold nanoparticle based dual platform with short DNA probe for the PCR free DNA biosensing using surface-enhanced Raman scattering. *Biosens. Bioelectron.* **2019**, *131*, 214−223.
(25) Xu, C.; Wang, X.; Zhu, J. W. Graphene metal particle nanocomposites. *J. Phys. Chem. C* **2008**, *112*, 19841−19845.
(26) Xu, C.; Chen, Z. X.; Fu, X. Z. Graphene oxide-mediated formation of freestanding, thickness controllable metal oxide films. *J. Mater. Chem.* **2011**, *21*, 12889−12893.
(27) Dou, Y. H.; Xu, J. T.; Ruan, B. Y.; Liu, Q. N.; Pan, Y. D.; Sun, Z. Q.; Dou, S. X. Atomic layer-by-layer Co_3O_4/graphene composite for high performance lithium-ion batteries. *Adv. Energy Mater.* **2016**, *6*, No. 1501835.
(28) Chen, H.; Müller, M. B.; Gilmore, K. J.; Wallace, G. G.; Li, D. Mechanically strong, electrically conductive, and biocompatible graphene paper. *Adv. Mater.* **2008**, *20*, 3557−3561.
(29) Guariguata, L.; Whiting, D.; Weil, C.; Unwin, N. The International Diabetes Federation diabetes atlas methodology for estimating global and national prevalence of diabetes in adults. *Diabetes Res. Clin. Pract.* **2011**, *94*, 322−332.
(30) Ogurtsova, K.; Da Rocha Fernandes, J. D.; Huang, Y.; Linnenkamp, U.; Guariguata, L.; Cho, N. H.; Cavan, D.; Shaw, J. E.; Makaroff, L. E. IDF diabetes atlas: global estimates for the prevalence of diabetes for 2015 and 2040. *Diabetes Res. Clin. Pract.* **2017**, *128*, 40−50.
(31) Mehdizadeh, T. S. M.; Soltani, M.; Samargandian, S.; Zarban, A.; Ebrahimzadeh, S. Comparison of glucose levels of the first and second fingertip blood drops in edematous diabetic patients hospitalized in intensive care units (point of care method). *Horiz. Med. Sci.* **2018**, *24*, 67−72.
(32) Siddiqui, S. A.; Zhang, Y.; Lloret, J.; Song, H.; Obradovic, Z. Pain-free blood glucose monitoring using wearable sensors: recent advancements and future prospects. *IEEE Rev. Biomed. Eng.* **2018**, *11*, 21−35.
(33) Zhang, W. J.; Du, Y. Q.; Wang, M. L. Noninvasive glucose monitoring using saliva nano-biosensor. *Sens. Bio-Sensing Res.* **2015**, *4*, 23−29.
(34) Yamaguchi, M.; Mitsumori, M.; Kano, Y. Noninvasively measuring blood glucose using saliva. *IEEE Eng. Med. Biol. Mag.* **1998**, *17*, 59−63.
(35) Jurysta, C.; Bulur, N.; Oguzhan, B.; Satman, I.; Yilmaz, T. M.; Malaisse, W. J.; Sener, A. Salivary glucose concentration and excretion in normal and diabetic subjects. *J. Biomed. Biotechnol.* **2009**, *2009*, No. 430426.
(36) Shanbhag, V. K. L.; Prasad, K. S. Graphene based sensors in the detection of glucose in saliva—a promising emerging modality to diagnose diabetes mellitus. *Anal. Methods* **2016**, *8*, 6255−6259.
(37) Soni, A.; Jha, S. K. A paper strip based non-invasive glucose biosensor for salivary analysis. *Biosens. Bioelectron.* **2015**, *67*, 763−768.
(38) Arakawa, T.; Kuroki, Y.; Nitta, H.; Chouhan, P.; Toma, K.; Sawada, S.; Takeuchi, S.; Sekita, T.; Akiyoshi, K.; Minakuchi, S.; Mitsubayashi, K. Mouthguard biosensor with telemetry system for monitoring of saliva glucose: A novel cavitas sensor. *Biosens. Bioelectron.* **2016**, *84*, 106−111.
(39) Das, D.; Kim, D. M.; Park, D. S.; Shim, Y. B. A glucose sensor based on an aminophenyl boronic acid bonded conducting polymer. *Electroanalysis* **2011**, *23*, 2036−2041.
(40) Chen, C.; Zhao, X. L.; Li, Z. H.; Zhu, Z. G.; Qian, S. H.; Flewitt, A. J. Current and emerging technology for continuous glucose monitoring. *Sensors* **2017**, *17*, 182−201.
(41) Wu, P.; Shao, Q.; Hu, Y. J.; Jin, J.; Yin, Y. J.; Zhang, H.; Cai, C. X. Direct electrochemistry of glucose oxidase assembled on graphene and application to glucose detection. *Electrochim. Acta* **2010**, *55*, 8606−8614.
(42) Zhou, D. L.; Feng, J. J.; Cai, L. Y.; Fang, Q. X.; Chen, J. R.; Wang, A. J. Facile synthesis of monodisperse porous Cu_2O nanospheres on reduced graphene oxide for non-enzymatic amperometric glucose sensing. *Electrochim. Acta* **2014**, *115*, 103−108.
(43) Espro, C.; Marini, S.; Giusi, D.; Ampelli, C.; Neri, G. Non-enzymatic screen printed sensor based on Cu_2O nanocubes for glucose determination in bio-fermentation processes. *J. Electroanal. Chem.* **2020**, *873*, No. 114354.
(44) Grujicic, D.; Pesic, B. Electrodeposition of copper: the nucleation mechanisms. *Electrochim. Acta* **2002**, *47*, 2901−2912.
(45) Qiao, F.; West, A. C. The impact of cations on nucleus density during copper electrodeposition. *Electrochim. Acta* **2014**, *150*, 8−14.

https://doi.org/10.1021/acsanm.1c00381
ACS Appl. Nano Mater. 2021, 4, 4790−4799

(46) Natter, H.; Hempelmann, R. Nanocrystaliine copper by pulsed electrodeposition: the effects of organic additives, bath temperature, and pH. *J. Phys. Chem. B* **1996**, *100*, 19525−19532.
(47) Nikolic, N.; Pavlovic, L.; Pavlovic, M.; Popov, K. Effect of temperature on the electrodeposition of disperse copper deposits. *J. Serb. Chem. Soc.* **2007**, *72*, 1369−1381.
(48) Radi, A.; Pradhan, D.; Sohn, Y. K.; Leung, K. T. Nanoscale shape and size control of cubic, cuboctahedral, and octahedral Cu-Cu_2O core-shell nanoparticles on Si(100) by one-step, templateless, capping-agent-free electrodeposition. *ACS Nano* **2010**, *4*, 1553−1560.
(49) Zhang, X. J.; Wang, G. F.; Liu, X. W.; Wu, H. Q.; Fang, B. Copper dendrites: synthesis, mechanism discussion, and application in determination of L-Tyrosine. *Cryst. Growth Des.* **2008**, *8*, 1430−1434.
(50) Taleb, A.; Xue, Y. P. Electrodeposition of self organized superstructure of copper dendrites or polyhedral particles on gold nanoparticle modified highly oriented pyrolytic graphite electrode. *Electrochim. Acta.* **2013**, *112*, 838−844.
(51) Fleisch, T. H. Reduction of copper oxides by UV radiation and atomic hydrogen studied by XPS. *Appl. Surf. Sci.* **1982**, *10*, 51−62.
(52) Park, J. Y.; Jung, Y. S.; Cho, J.; Choi, W. K. Chemical reaction of sputtered Cu film with PI modified by low energy reactive atomic beam. *Appl. Surf. Sci.* **2006**, *252*, 5877−5891.
(53) Diaz-Droguett, D. E.; Espinoza, R.; Fuenzalida, V. M. Copper nanoparticles grown under hydrogen: study of the surface oxide. *Appl. Surf. Sci.* **2011**, *257*, 4597−4602.
(54) Wu, S. C.; Tan, C. S.; Huang, M. H. Strong facet effects on interfacial charge transfer revealed through the examination of photocatalytic activities of various Cu_2O-ZnO heterostructures. *Adv. Funct. Mater.* **2017**, *27*, No. 1604635.
(55) Zhen, W.; Jiao, W.; Wu, Y.; Jing, H.; Lu, G. The role of a metallic copper interlayer during visible photocatalytic hydrogen generation over a $Cu/Cu_2O/Cu/TiO_2$ catalyst. *Catal. Sci. Technol.* **2017**, *7*, 5028−5037.
(56) Turner, A.; Karube, I.; Wilson, G. S. *Biosensors: Fundamentals and Applications*; Oxford University Press: Oxford, 1987.
(57) Lee, W. C.; Kim, K. B.; Gurudatt, N. G.; Hussain, K. K.; Choi, C. S.; Park, D. S.; Shim, Y. B. Comparison of enzymatic and non-enzymatic glucose sensors based on hierarchical Au-Ni alloy with conductive polymer. *Biosens. Bioelectron.* **2019**, *130*, 48−54.
(58) Cao, H. M.; Yang, A. L.; Li, H.; Wang, L. L.; Li, S. P.; Kong, J. L.; Bao, X. C.; Yang, R. Q. A non-enzymatic glucose sensing based on hollow cuprous oxide nanospheres in a Nafion matrix. *Sens. Actuators, B* **2015**, *214*, 169−173.
(59) Li, K.; Fan, G. L.; Yang, L.; Li, F. Novel ultrasensitive non-enzymatic glucose sensors based on controlled flower-like CuO hierarchical films. *Sens. Actuators, B* **2014**, *199*, 175−182.
(60) Meng, L.; Jin, J.; Yang, G. X.; Lu, T. H.; Zhang, H.; Cai, C. X. Nonenzymatic electrochemical detection of glucose based on palladium-single-walled carbon nanotube hybrid nanostructures. *Anal. Chem.* **2009**, *81*, 7271−7280.
(61) Veetil, J. V.; Jin, S.; Ye, K. A glucose sensor protein for continuous glucose monitoring. *Biosens Bioelectron.* **2010**, *26*, 1650−1655.
(62) Gupta, S.; Nayak, M. T.; Sunitha, J. D.; Dawar, G.; Sinha, N.; Rallan, N. S. Correlation of salivary glucose level with blood glucose level in diabetes mellitus. *J. Oral Maxillofac. Pathol.* **2017**, *21*, 334−339.
(63) Zhou, X. M.; Nie, H. G.; Yao, Z.; Dong, Y. Q.; Yang, Z.; Huang, S. M. Facile synthesis of nanospindle-like Cu_2O/straight multi-walled carbon nanotube hybrid nanostructures and their application in enzyme-free glucose sensing. *Sens. Actuators, B* **2012**, *168*, 1−7.
(64) Fan, H. H.; Weng, W. L.; Lee, C. Y.; Liao, C. N. Electrochemical cycling-induced spiky Cu_xO/Cu nanowire array for glucose sensing. *ACS Omega* **2019**, *4*, 12222−12229.
(65) Li, R.; Liu, X.; Wang, H.; Wu, Y.; Chan, K. C.; Lu, Z. Sandwich nanoporous framework decorated with vertical CuO nanowire arrays for electrochemical glucose sensing. *Electrochim. Acta* **2019**, *299*, 470−478.
(66) Wang, A. J.; Feng, J. J.; Li, Z. H.; Liao, Q. C.; Wang, Z. Z.; Chen, J. R. Solvothermal synthesis of Cu/Cu_2O hollow microspheres for non-enzymatic amperometric glucose sensing. *CrystEngComm* **2012**, *14*, 1289−1295.
(67) Xiao, F.; Li, Y.; Gao, H.; Ge, S.; Duan, H. Growth of coral-like PtAu-MnO_2 binary nanocomposites on free-standing graphene paper for flexible nonenzymatic glucose sensors. *Biosens. Bioelectron.* **2013**, *41*, 417−423.
(68) Liu, M.; Liu, R.; Chen, W. Graphene wrapped Cu_2O nanocubes: non-enzymatic electrochemical sensors for the detection of glucose and hydrogen peroxide with enhanced stability. *Biosens. Bioelectron.* **2013**, *45*, 206−212.
(69) Zhang, W. J.; Du, Y. Q.; Wang, M. L. On-chip highly sensitive saliva glucose sensing using multilayer films composed of single-walled carbon nanotubes, gold nanoparticles, and glucose oxidase. *Sens. Bio-Sensing Res.* **2015**, *4*, 96−102.
(70) Dong, C.; Zhong, H.; Kou, T.; Frenzel, J.; Eggeler, G.; Zhang, Z. Three-dimensional Cu foam-supported single crystalline mesoporous Cu_2O nanothorn arrays for ultra-highly sensitive and efficient nonenzymatic detection of glucose. *ACS Appl. Mater. Interfaces* **2015**, *7*, 20215−20223.

https://doi.org/10.1021/acsanm.1c00381
ACS Appl. Nano Mater. 2021, 4, 4790−4799